

Region-level Active Learning for Cluttered Scenes

Michael Laielli, Giscard Biamby, Dian Chen, Adam Loeffler,
Phat Dat Nguyen, Ross Luo, Trevor Darrell, Sayna Ebrahimi
UC Berkeley

{laielli,gbiamby,dian,aross.1311,phatdatn,ross.luo,trevordarrell,sayna}@berkeley.edu

Abstract

Active learning for object detection is conventionally achieved by applying techniques developed for classification in a way that aggregates individual detections into image-level selection criteria. This is typically coupled with the costly assumption that every image selected for labelling must be exhaustively annotated. This yields incremental improvements on well-curated vision datasets and struggles in the presence of data imbalance and visual clutter that occurs in real-world imagery. Alternatives to the image-level approach are surprisingly under-explored in the literature. In this work, we introduce a new strategy that subsumes previous Image-level and Object-level approaches into a generalized, Region-level approach that promotes spatial-diversity by avoiding nearby redundant queries from the same image and minimizes context-switching for the labeler. We show that this approach significantly decreases labeling effort and improves rare object search on realistic data with inherent class-imbalance and cluttered scenes.

1. Introduction

Training a visual object detector often requires massive amounts of bounding box labels in order to achieve desired performance levels. This data is expensive to collect since the labeling process requires multiple stages of exhaustive searches for the presence of multiple categories and instances. Active learning is an attractive mitigation strategy that aims to label only the most informative samples, achieving a desired performance with less labels. However, applying active learning to visual object detection is not straightforward.

Existing active learning strategies for object detection fall into two distinct approaches. The first, and most prevalent in the literature, takes an *Image-level* approach that sends a query to the “oracle” labeler in the form of a whole-image for exhaustive labeling, typically selected based on object prediction scores aggregated within each image [17, 6, 2].

While this minimizes the total number of images scanned, it is vulnerable to intra-image redundancy: objects within the same image are likely to be similar and therefore redundant in terms of little-to-no added information. The second approach takes an *Object-level* approach, foregoing exhaustive labeling and sending a single-object query to the oracle [23, 8]. This approach increases diversity by breaking the exhaustive labeling assumption, but incurs several costs such as introducing many false negatives to the labeled pool of images, increasing visual search, and maximizing context switching required of the labeler.

In this work, we propose ReAL, a *Region-level* Active Learning approach that selects regions of high informativeness that contain diverse groups of objects while minimizing the query area. ReAL, depicted in Figure 2, finds region-level queries by first considering the *similarity* of neighboring object predictions. Then, it incrementally expands the query region for each nearby prediction that is found to have low cosine-similarity between feature embeddings from the detection model.

ReAL is agnostic to both the scoring function and the selection strategy, and is thus easily applied to typical active learning methods comprised of a scoring function, selection strategy, or both. Our approach avoids label redundancy without drastically increasing false negatives or total pixels scanned by not being constrained to either extreme of image- or object-level fixed approaches.

In the extreme cases of images densely packed with large objects or sparsely, with small objects, ReAL can become equivalent to the Image- or Object-level approaches, respectively.

We evaluate ReAL against the Image-level and Object-level baselines with a suite of previously reported Active Learning for detection methods. We additionally present a novel extension of a recent Minimal Active Learning [10] method to handle the detection setting, which we call D-MAL, and which incorporates both uncertainty and diversity as measures of informativeness for detection active learning.

We run our evaluation across two distinct datasets: The

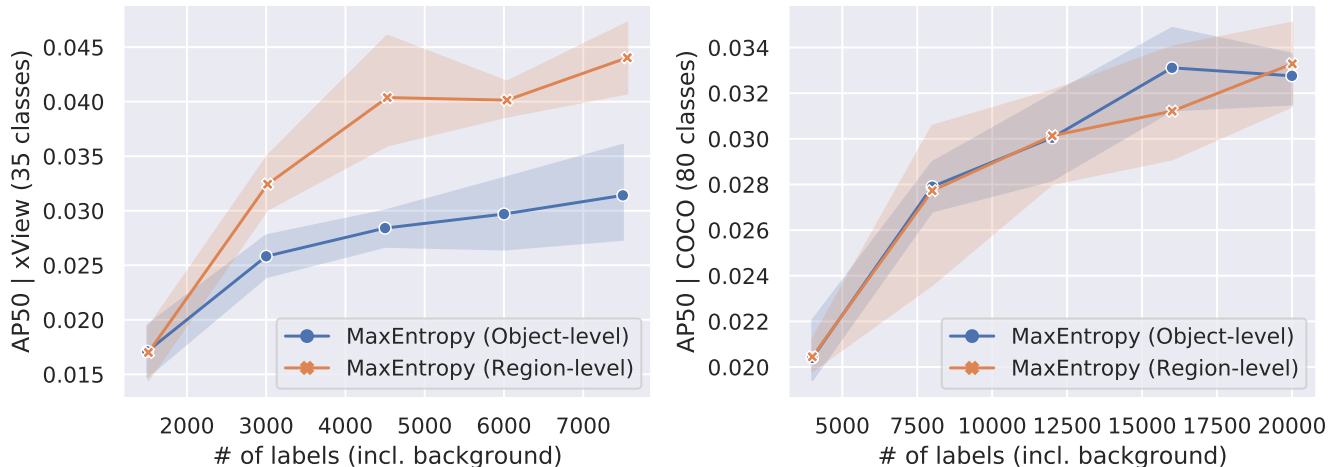


Figure 1: xView (left) and COCO (right) AP50 results for five splits in terms of the total labels applied by the oracle including background instances. We count mistakenly queried background instances towards the labeling budget since the oracle must verify that no object exists in that particular image region. Our ReAL approach significantly boosts the performance of entropy-based methods in realistically cluttered scenes (xView) over an Object-level approach. Performance is low for both datasets since we’re evaluating with relatively few instances per class and no data augmentation.

classic object detection benchmark COCO 2017 with relatively low object clutter, and the realistic xView dataset of satellite imagery containing highly varying levels of object clutter, class imbalance, and label noise. The latter are characteristics rarely encountered in more traditionally curated vision datasets. We first confirm that ReAL and Object-level performs similarly on COCO 2017, as expected due to the high informativeness of all objects and low levels of clutter due to heavy dataset curation. On the xView dataset our ReAL approach dynamically finds image regions with diverse, high-entropy objects to reduce the labeling effort by up to 60% as compared to Object-level and Image-level approaches with an entropy-based method. We also empirically show that ReAL combined with our novel D-MAL method outperforms the all baseline approaches across multiple methods in terms of detection accuracy and object search with relative improvements of up to 24% and 41%, respectively.

2. Related Work

Although active learning for object detection is a long-standing problem [1, 13, 5, 7], it has remained relatively under-explored compared to image classification [21, 10, 4, 18, 22, 25, 16, 3, 11, 24]. Sampling strategies developed in the literature either request for full-image annotations [17, 6, 2] or select individual objects to be labeled [23, 8].

Image-level approaches often follow algorithms that were originally proposed for classification settings where they aggregate results computed for different instances in an image to decide whether or not an image should be labeled.

Roy et al. [17] used a query by committee approach [20] to query the image with the largest disagreement between the convolutional layers in the object detector backbone. Brust et al. [6] used uncertainty measures on detected bounding boxes to compute a per-image aggregated score. Aghdam et al. [2] proposed an Image-level score that accumulated pixel-level importance scores such that an image with the highest number of false-positive and false negative predictions would be sent to the oracle. Desai et al. [9] proposed an adaptive learning strategy where at each cycle, they first used weakly-labeled data received from the labeler to optimize the model and then switched to a stronger form of supervision as required when further training the model. Kao et al. [12] proposed two metrics to measure object informativeness including ‘localization tightness’ and ‘localization stability’ where the former is based on the overlapping ratio between the region proposal and the final prediction and the latter is based on the variation of predicted object locations when input images are corrupted by noise.

Instance-level methods were introduced to mitigate the costs of full-frame labeling in Image-level strategies. Wang et al. [23] proposed a Self-supervised Sample Mining using pseudo-labeling for enhancing the object detector via the introduced cross image validation, i.e., pasting these proposals into different labeled images to comprehensively measure their values under different image contexts. Desai et al. [8] used two metrics for querying bounding boxes to be labeled including uncertainty associated with classification predictions and coreset method [18] that computed distance based on bounding box feature representations.

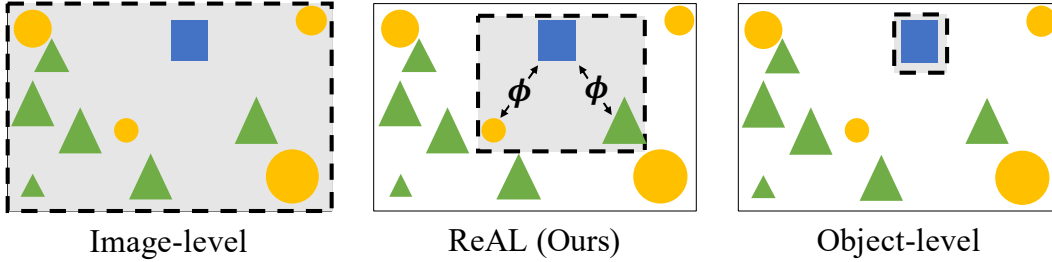


Figure 2: Conceptual illustration of our proposed method, Region-level Active Learning (ReAL), which identifies dense regions of informativeness for querying the oracle by dynamically expanding to include dissimilar neighboring object predictions. ReAL builds a query region around an initial query prediction (blue) by expanding the region boundaries (dotted black) to include informative neighbor predictions (yellow, green) with low similarity, ϕ . In contrast to the Image-level approach, ReAL avoids querying redundant instances of common objects. It also mitigates the main drawback of Object-level sampling by reducing false-negatives, minimizing visual search, and capturing scene context.

ReAL breaks the fixed-level constraints of Image- and Object-level approaches by introducing the notion of dynamic query areas in the image to include any number of potential object predictions.

3. Region-level Active Learning (ReAL)

In this section, we introduce ReAL, a generalized active learning approach for object detection that prioritizes the labeling of information-dense regions over single instances or sparse swaths.

We consider the problem of learning a label-efficient model by iteratively selecting the most *informative* object predictions from a given *split* to be labeled by an oracle which is usually a human expert.

We start with an initial small pool of images denoted as $\mathcal{L} = \{(x_L^i, y_L^i)\}_{i=1}^{N_L}$, where $y_L^i = \{O_j\}_{j=1}^{M_i}$ is the set of annotations of each image. For a known, fully-annotated dataset, the initial pool is constructed by randomly sampling from all available annotations, and taking all the images associated with the annotations. Specifically, for each category we uniformly sample $p\%$ of all its annotations, with a hard cap k on the number of instances. This reflects our prior knowledge of a dataset, i.e., we have more access to the more common categories whereas less to the rarer categories, while avoiding exhausting any category in the beginning. The remaining images constitute the large pool of unlabeled data, which is denoted as $\mathcal{U} = \{x_U^i\}_{i=1}^{N_U}$ where our goal is to populate a fixed sampling *budget* per object category, b , using an acquisition strategy to query instances from the unlabeled pool ($x_U \sim X_U$) such that the expected loss is minimized.

After an initial labeled pool of images has been established, ReAL can proceed, given any active learning method comprised of a scoring function, I , that attempts to convey the *informativeness* of the given query to the model, selec-

tion strategy, or both. ReAL makes full use of the detection model by taking all predicted bounding boxes on the labeled pool as input. Given each bounding box prediction by the model and corresponding informativeness score, ReAL defines a larger region, defined in detail in the next subsection.

3.1. Initial maximum area

Our approach starts by defining an initial maximum area for each prediction made by the detection model on the unlabeled images. The boundaries of this area are defined as

$(x_{\min}, y_{\min}, x_{\max}, y_{\max})$ and based on the width, w_b , and height, h_b , of the predicted box, b . $(x_{b,\min}, x_{b,\max}, y_{b,\min}, y_{b,\max})$ are the boundaries of the predicted box.

$$\begin{aligned}
 x_{\min} &= \max(0, x_{b,\min} - \alpha_w w_b) \\
 x_{\max} &= \min(w_{img}, x_{b,\max} + \alpha_w w_b) \\
 y_{\min} &= \max(0, y_{b,\min} - \alpha_h h_b) \\
 y_{\max} &= \min(h_{img}, y_{b,\max} + \alpha_h h_b)
 \end{aligned} \tag{1}$$

where α expands the area proportionally to the predicted box size such that the area becomes multiple times the size of small object predictions and only slightly expands for the largest predictions. The width and height components of α are defined as

$$\begin{aligned}
 \alpha_w &= \beta \left(1 - \frac{w_b}{w_{img}}\right)^\beta \\
 \alpha_h &= \beta \left(1 - \frac{h_b}{h_{img}}\right)^\beta
 \end{aligned} \tag{2}$$

where the ratio of object size w_b to image size w_{img} is subtracted from 1. The resulting ratio, inversely proportional to object size, is then raised to and multiplied by β . The β parameter represents the number of times by which the boundaries of the smallest valid box size should be extended. For

example, a small box should yield a box-image ratio close to zero, thus $\alpha_{w,h}$ ends up close to the full value of β .

3.2. Informative neighbors

Once an initial maximum area, $(x_{\min}, y_{\min}, x_{\max}, y_{\max})$, has been established, ReAL searches through the object predictions that intersect the area. Formally, we consider all the contained predictions as the maximum region set, \mathcal{R}_{\max} . In ascending order by distance to the query, we compute a score, $\Phi(\cdot)$, based on cosine similarity, between a particular neighbor, the query prediction, and other previously accepted neighbors. If the score meets a threshold, it is added to the true region set, \mathcal{R} .

$$\mathcal{R} = \{n \in \mathcal{R}_{\max} | \Phi(n) > \gamma\} \quad (3)$$

where manually decreasing γ enforces more dissimilarity on the region. In our experiments, we set $\gamma = 0.5$. The similarity scoring function, $\Phi(\cdot)$, considers the cosine similarity, $\phi(\cdot)$, between a given neighbor and the set of all previously accepted neighbors, \mathcal{R}_{prev} , including the query.

$$\Phi(n_i) = \frac{1}{|\mathcal{R}_{prev}|} \sum_{n_i \in \mathcal{R}_{prev}} \phi(q, n) \quad (4)$$

3.3. Region Scores

Once a region of dissimilar predictions has been established we shrink its corresponding pixel boundaries down to the minimum bounding box containing all the accepted neighbors. Then the region is scored according to an accumulation of the uncertainty, similarity, and overlap of each query-neighbor pairing. The elemental scoring function is

$$S_n(q, n) = I(n)(1 - \phi(q, n)) \quad (5)$$

where $I(\cdot)$ is an informativeness measure, such as entropy, of the neighboring prediction. The second term subtracts the cosine similarity between query, q and neighbor, n from 1 to reduce the score in the case of high similarity.

The final score, $S_{\mathcal{R}}$, is the sum of the scoring function applied to each query-neighbor pair, weighted by the informativeness of the query prediction.

$$S_{\mathcal{R}}(q, \mathcal{R}) = I(q) \sum_{n \in \mathcal{R}} S_n(q, n) \quad (6)$$

4. Minimax Active Learning for Detection (D-MAL)

In this section, we describe our novel extension of the Minimax Active Learning method (MAL) [10] for object detection, D-MAL, depicted in Figure 3. MAL is a semi-supervised active learning method which is originally introduced for classification and segmentation. It has the ability

to query samples based on uncertainty using entropy and/or diversity using a classifier that is designed to discriminate the most *different* samples from those already seen in the feature space. We use this method to analyze the uncertainty and diversity role in active learning for object detection in conjunction with our /method approach (see Section 5.2).

Figure 3 illustrates D-MAL architecture for detection which has three major building blocks: **(i)** a feature encoder (F) that attempts to minimize the entropy of the unlabeled data for better clustering. **(ii)** a distance-based classifier head that adversarially learns per-object weight vectors as prototypes and attempts to maximize the entropy of the unlabeled data **(iii)** a *labeledness* head that takes the extracted ROI features as input and predicts which pool each object belongs to. D-MAL leverages both the labeled and unlabeled objects by performing the minimax entropy optimization in a semi-supervised learning fashion which is easy to train and does not require labels.

The intuition behind D-MAL is that while the feature extractor minimizes the entropy by pushing the unlabeled objects to be clustered near the prototypes, the classifier increases the entropy of the unlabeled objects, and hence makes them similar to all class prototypes. On the other hand, they both learn to classify the labeled objects using a cross-entropy loss, enhancing the feature space with more discriminative features. We train the *labeledness* head along with the classifier and the box regressor heads to predict *labeledness* for each box. In an Object-level approach, D-MAL queries objects which (i) are predicted as unlabeled with high confidence by the *labeledness* head and (ii) achieved high entropy by the classifier will be sent to the oracle. In ReAL approach however, the labeledness and entropy scoring functions area used as a basis to find and score multi-object regions. These scores are combined with measures of similarity between region-level boxes that are computed as the cosine similarity between normalized feature embeddings extracted from the Faster-RCNN model by the ROI Feature Extractor depicted in Figure 3.

5. Experimental setup

In this section we review the details of our experimental setting, benchmark datasets, and baselines used in our evaluation as well as the implementation details.

5.1. Datasets

We have evaluated our ReAL approach on **xView** [14] as one of the largest publicly available datasets of overhead imagery, as well as **COCO 2017**, [15] which is a common object detection benchmark. Below we describe the qualities of xView that make it a good benchmarking set for Active Learning for cluttered scenes and contrast it with COCO 2017. We also provide details on pre-processing, choice of performance metrics, and training

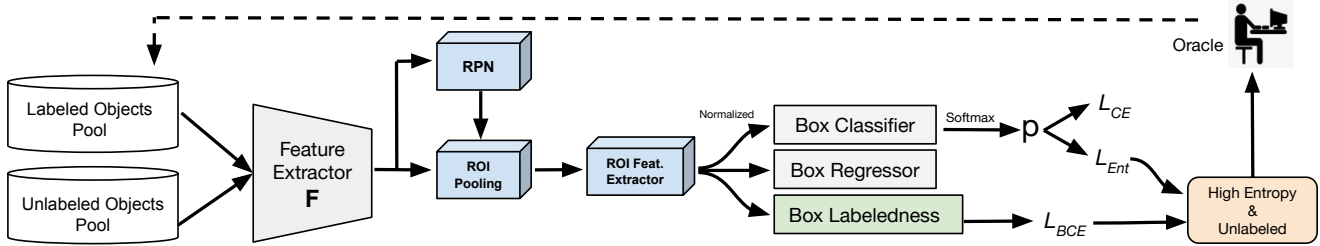


Figure 3: Our D-MAL pipeline using a Faster-RCNN detector. Both labeled and unlabeled data feed into the Faster-RCNN’s backbone architecture F as the feature extractor. We have added an extra head to the original Faster-RCNN architecture which is trained to predict *labeledness* which refers to whether an object has been labeled or not. The original classifier head is also replaced with a normalization layer followed by a cosine similarity-based classifier C which is trained to maximize entropy on unlabeled objects, whereas F is trained to minimize it. We have evaluated D-MAL with Image-level, Object-level, and our proposed Region-level selection strategies.

hyper-parameters for both datasets. License and privacy details for xView and COCO 2017 are discussed in [14, 15].

xView [14]. xView consists of 846 large satellite images that range from 2500 to 3500 pixels². 60 classes of objects are exhaustively labeled with bounding boxes for a total of $\sim 1\text{M}$ labeled object instances. The class-level breakdown of these instances follows a long-tail distribution, with two categories numbering in the hundreds of thousands, and many others in the hundreds or even tens. By comparison, all categories of the COCO 2017 dataset have at least 1000 instances.

Data pre-processing for xView. In our experiment, we make some adjustments to the xView dataset for the purposes of data processing and evaluation. First, we join some child classes so that low-shot categories have enough instances for robust evaluation, which yields 35 total object categories. Second, we break the large images into smaller 512×512 tiles so that the small batches will fit in GPU memory during training. Our version has 19,631 image tiles of size 512×512 and 418,217 total labels in the train set and 6,910 tiles and 158,811 labels in the validation set.

xView clutter and imbalance. Our version of xView retains the drastic data imbalance and clutter with the top two categories containing over 100,000, 23 categories containing less than 1,000, and 7 categories containing less than 100 instances. With 20.6 objects on average, the image tiles of xView appear highly cluttered compared to the COCO 2017 dataset which has 7.7 objects on average spread across larger images. xView image tiles also reach a much higher *maximum* clutter compared to COCO 2017. Whereas COCO 2017 images cap out at 15 object per image, xView image tiles reach drastically higher levels of density: The top-10% of xView image tiles contain an average of 101 objects and the most cluttered image tiles in xView contain over 500 objects.

COCO 2017 [15] We use the 2017 version of COCO which

consists of 118,287 images and 860,001 objects in the training set, and 5,000 images and 36,781 objects in the test set. On average, the COCO dataset contains 7.7 object instances per image. This amount is less than would naturally occur since the strategies employed in the dataset curation explicitly avoided annotating more than 10-15 object instances within a single image [15]. During training and testing, we resize the images with a minimum short side 704 and a maximum long side 1333 while keeping the aspect ratio.

Performance measurement. We measure the performance on the xView and COCO 2017 datasets by calculating the Average Precision (AP) at an IoU threshold of 0.5. This moderate threshold level is preferred over the stricter 0.75 or 0.5 : 0.95 thresholds because it is less sensitive to minuscule box shifts at the scale of the smallest object sizes in both datasets. Both datasets are evaluated in low data regimes in the early splits, e.g. 100 labels per category, and a less stringent metric allows for better differentiation in challenging conditions.

Object detector architecture and training details. All model-based methods (D-MAL, entropy, and model-based random) for all approaches use a Faster-RCNN detector with a ResNet-50 backbone with Feature Pyramid Network (FPN). With the first two layers frozen, each FRCNN model is trained on a GeForce RTX 2080 Ti (11GB). All experiments are trained 5 times with unique random seeds and the mean reported. The COCO 2017 experiments were trained for 30 epochs with a batch size of 2, learning rate 0.01, using an SGD optimizer. The learning rate is reduced by 0.1 at 22 and 28 epochs. The xView experiments were trained for 30 epochs with a batch size of 4, learning rate 0.01, using an SGD optimizer. The learning rate is reduced by 0.1 at 25 and 28 epochs.

In our experiments, we use four active learning methods among the three approaches. These methods vary in

their scoring functions and selection strategies to include informativeness scores such as *Entropy* and *Labeledness*, and also employ different selection criteria such as random and based on one or more types of informativeness scores. We briefly describe each active learning method below and provide more approach-specific details in the next section, 5.2.

1. **Minimax Active Learning for Detection (D-MAL).** We use our novel extension of MAL for object detection which was described in Section 4.
2. **Maximum Entropy (MaxEnt)** [19] prioritizes objects with the highest entropy (in the Object-level approach) or images with the highest aggregated entropy score (in the Image-level approach) to be labeled.
3. **Model-based Random (ModelRand)** randomly selects from the set of all objects predicted by the detection model trained on the labeled pool of images. Note that no score is computed or employed in this method. Despite its simplicity, model-based random selection is surprisingly hard to beat in many active learning benchmarks. We use this baseline for only the Object-level and ReAL approaches, as this form of model-based random sampling of individual object predictions is not applicable to the Image-level approach.
4. **Model-free Random (Random)** *purely random* selection strategy used for the Image-level approach. Without any model input, images are selected at random for exhaustive labeling.

5.2. Active learning approaches setup

In this section, we describe the setup of the two baseline approaches Image-level and Object-level, and our proposed Region-level approach, ReAL. For each approach, we describe the oracle querying process, including any relevant distinctions between active learning selection methods to which the approaches are applied.

Image-level. The Image-level approach selects one image at a time to be exhaustively labeled by the oracle until the budget in terms of individual labels is reached, marking the end of a single *split*. Each model-based selection method computes an Image-level informativeness score based on the object predictions made by the respective model. No score is computed for the Random baseline method. While the informativeness scores at the object level may differ across methods, the Image-level aggregation method is the same: we take the mean of all object informativeness scores to get a single Image-level score. The baseline methods evaluated in the Image-level approach are: Maximum Entropy, and Random.

Object-level. The Object-level approach selects one predicted object instance at a time to be labeled by the oracle. A label is only returned if a ground-truth instance of any category exists in its location that has any Intersection-over-Union (IoU) score of 0.25, or greater, with the predicted query box. If there are multiple ground truth boxes intersecting the query, then the one with the highest IoU with the ground truth is selected regardless of the predicted category of the query. For each Object-level query to the oracle, one of two interactions occurs: either a ground-truth bounding box label is returned, or the oracle determines that no ground-truth bounding box label exists in the location of the predicted query box and no label is returned. Without accounting for the latter type of interaction, a vastly inefficient random query predictor would falsely exhibit comparable performance to a model that randomly selected among accurate predictions, hiding the fact that it could require orders of magnitude more interactions. The baseline methods evaluated in the Object-level approach are: Maximum Entropy, and Model-random. Maximum Entropy is essentially the same as in Image-level, but without the Image-level aggregation. Each predicted object in the unlabeled pool is ranked and sent as queries to the oracle in order of descending predicted informativeness. Model-random selects randomly shuffled predictions made on the unlabeled pool to send as queries.

Region-level. Our proposed Region-level approach, ReAL, selects one image region at a time to be labeled by the oracle. A single *region* can encompass any single rectangular area within an image including, but not limited to, a single object or the entire image. The oracle returns all ground truth labels which are at least 25% covered by the region query box, regardless of the predicted category of the query. The budget is measured in terms of ground truth objects labeled by the oracle as well as region queries that yield zero groundtruth objects. The methods evaluated in the Region-level approach are: D-MAL, Maximum Entropy, and Model-random. The region scores are computed according to Section 3. Each region found in the unlabeled pool is ranked according the respective selection method’s ranking algorithm and sent to the oracle for labeling in descending order.

6. Results

In this section, we present and discuss our results for all three approaches: ReAL, Image-level, and Object-level, and methods: D-MAL, Maximum Entropy, ModelRandom and Random.

xView. In this experiment we evaluate performance on the realistically challenging xView dataset [14]. The ReAL approach makes a significant improvements in terms of both Average Precision (AP50) and object search (Labeled

Table 1: Active learning performance results across approaches and methods on the xView dataset. We use a budget of 1500 labels (initial and otherwise) and report the mean across five seeds with standard deviation in parentheses. ReAL outperforms across all splits for both the Maximum Entropy (MaxEnt) and D-MAL methods.

Approach (Method)	Split 0	Split 1	Split 2	Split 3	Split 4
<i>Init. budget: 1500, Budget: 1500</i>	AP50 (STD)	AP50 (STD)	AP50 (STD)	AP50 (STD)	AP50 (STD)
Image-level (Random)	.017 (.003)	.020 (.003)	.024 (.002)	.020 (.003)	.024 (.002)
Image-level (MaxEnt)	.017 (.003)	.020 (.003)	.022 (.002)	.031 (.002)	.037 (.002)
Object-level (ModelRand)	.017 (.003)	.029 (.002)	.034 (.002)	.039 (.004)	.037 (.003)
Object-level (MaxEnt)	.017 (.003)	.026 (.002)	.028 (.002)	.030 (.004)	.031 (.005)
ReAL (ModelRand)	.017 (.003)	.030 (.002)	.035 (.002)	.037 (.003)	.037 (.003)
ReAL (MaxEnt)	.017 (.003)	.032 (.003)	.040 (.006)	.040 (.002)	.044 (.004)
ReAL (D-MAL)	.028 (.001)	.037 (.003)	.042 (.004)	.041 (.002)	.046 (.002)

Table 2: Performance on the top-10 (most common), middle-10, and bottom-10 (rarest) category groupings in terms of total instances in the xView dataset. ReAL outperforms the baselines across all splits in the middle-10 and rarest categories in terms of accuracy (AP50) and object search (Labeled %).

Approach (Method)	Split 0	Split 1	Split 2	Split 3	Split 4
<i>Top-10 categories</i>	AP50 / Labeled %	AP50 / Labeled %	AP50 / Labeled %	AP50 / Labeled %	AP50 / Labeled %
Image-level (Random)	0.005 / 1.76	0.015 / 2.15	0.025 / 2.53	0.041 / 2.85	0.049 / 3.23
Image-level (MaxEnt)	0.006 / 1.76	0.011 / 2.14	0.02 / 3.05	0.039 / 4.23	0.051 / 5.24
Object-level (ModelRand)	0.005 / 1.76	0.015 / 2.41	0.021 / 2.91	0.023 / 3.39	0.024 / 3.79
Object-level (MaxEnt)	0.005 / 1.76	0.015 / 2.59	0.019 / 2.91	0.019 / 3.17	0.023 / 3.4
ReAL (ModelRand)	0.005 / 1.76	0.018 / 2.73	0.023 / 3.43	0.03 / 4.32	0.032 / 4.93
ReAL (MaxEnt)	0.005 / 1.76	0.017 / 4.01	0.027 / 5.75	0.032 / 6.88	0.042 / 7.79
ReAL (D-MAL)	0.011 / 1.76	0.013 / 3.36	0.015 / 4.71	0.017 / 5.74	0.019 / 6.57
<i>Middle-10 categories</i>					
Image-level (Random)	0.043 / 7.53	0.048 / 7.92	0.052 / 8.2	0.057 / 8.62	0.062 / 8.95
Image-level (MaxEnt)	0.042 / 7.53	0.045 / 8.19	0.05 / 9.18	0.061 / 10.57	0.071 / 12.5
Object-level (ModelRand)	0.041 / 7.53	0.067 / 10.69	0.076 / 11.95	0.08 / 13.14	0.081 / 14.2
Object-level (MaxEnt)	0.043 / 7.53	0.057 / 9.76	0.064 / 10.9	0.062 / 11.65	0.066 / 12.26
ReAL (ModelRand)	0.042 / 7.53	0.069 / 10.36	0.076 / 11.5	0.082 / 12.67	0.084 / 13.63
ReAL (MaxEnt)	0.042 / 7.53	0.068 / 12.46	0.08 / 14.87	0.083 / 16.79	0.086 / 17.88
ReAL (D-MAL)	0.066 / 7.53	0.079 / 13.11	0.087 / 16.3	0.088 / 18.42	0.091 / 19.96
<i>Bottom-10 categories</i>					
Image-level (Random)	0.001 / 20.2	0.001 / 20.45	0.002 / 20.66	0.003 / 20.94	0.002 / 21.28
Image-level (MaxEnt)	0.001 / 20.2	0.002 / 21.78	0.002 / 24.74	0.004 / 28.03	0.005 / 31.49
Object-level (ModelRand)	0.001 / 20.2	0.005 / 26.77	0.008 / 27.62	0.011 / 28.41	0.009 / 29.09
Object-level (MaxEnt)	0.001 / 20.2	0.005 / 27.46	0.006 / 28.98	0.007 / 29.8	0.009 / 30.75
ReAL (ModelRand)	0.001 / 20.2	0.005 / 23.03	0.004 / 25.16	0.005 / 27.2	0.006 / 28.9
ReAL (MaxEnt)	0.001 / 20.2	0.005 / 29.43	0.008 / 33.48	0.01 / 37.34	0.009 / 40.18
ReAL (D-MAL)	0.01 / 20.2	0.016 / 31.49	0.019 / 36.04	0.015 / 38.4	0.022 / 40.16

%) over Image-level and Object-level approaches. Figure 1 demonstrates that the ReAL approach can drastically improve the performance of a model-based uncertainty method by reaching a 42% improvement over the Object-level baseline (.031 to .044). Furthermore, ReAL achieves similar performance within the first split compared to what Object-level achieves by the final split i.e. ReAL

can match the performance of Object-level with 60% less labeling effort by the oracle. We see a striking difference in performance of the active learning approaches between xView and COCO 2017. While ReAL performs similar to the baseline on COCO 2017, it significantly outperforms on xView, where heavy object clutter and class imbalance are prevalent, showing that new strategies are needed for real-

istic data settings and motivating our ReAL approach.

Table 1 shows the performance of all approaches and methods on the xView benchmark. The ReAL approach outperforms across all splits for both the Maximum Entropy (MaxEnt) and D-MAL methods. In the final split, ReAL (D-MAL) improves over the strongest baseline, Object-level (ModelRand), by a 24% relative increase in AP50 (.037 to .046). Furthermore, ReAL (D-MAL) reduces the labeling effort by up to 50% considering it takes Object-level (ModelRand) until Split 3 to reach the accuracy achieved by ReAL (D-MAL) in Split 1.

Table 2 breaks down the performance results into the top-10 most common, bottom-10 rarest, and middle-10 categories in the xView dataset. The ReAL approach completely outperforms the baselines in the middle-10 and rarest categories in terms of accuracy (AP50). ReAL (D-MAL) shows a relative improvement over the strongest baseline of 12.3% in the middle-10 categories and 133% in the rarest categories. The Image-level approach remains unbeaten in only the final two splits of the top-10 most common categories. In terms of object search (% of instances found and labeled out of all category instances in the dataset), ReAL outperforms across the most common, middle-10, and rarest category breakdowns for both the Maximum Entropy (MaxEnt) and D-MAL methods. ReAL (MaxEnt) finds 8.7% more rare objects (a 28% relative increase) over the strongest baseline (Image-level MaxEnt) in the last split. In the middle-10 categories, ReAL (D-MAL) finds 5.8% more objects (a 41% relative increase) over the strongest baseline, Object-level (ModelRand), in the last split. Surprisingly, even in the most common categories, ReAL finds a higher percentage of the total instances in the dataset. This can be explained by Image-level spending almost all of its labeling budget on the top-2 most common categories, *buildings* and *cars* which outnumber the other most common categories by an order-of-magnitude. By exhaustively labeling all objects in each selected image, it cannot avoid oversampling these two categories. ReAL avoids this pitfall and more than makes up the difference in the remaining 8 most common categories. In other words, Image-level casts *too large of a net* and this matters when there is heavy category imbalance as in xView. Conversely, Object-level casts *too small of a net*. While Object-level has the ability to query more images in total, it suffers from wasting its budget on many unsuccessful queries. ReAL outperforms by *adapting the size of the net* to carefully subsample from regions of high uncertainty and/or diversity while lowering the risk of unsuccessful queries.

COCO 2017. The results for COCO are shown in Figure 1. Performance on the COCO 2017 benchmark is nearly indistinguishable between Object-level and ReAL. This is somewhat expected since COCO is significantly less cluttered and more balanced across categories than the less-curated

xView. This was our motivation for evaluating on the xView dataset with minimal pre-selection and highly cluttered images.

7. Discussion and conclusion

Our ReAL approach is limited to the object detection setting with 2D bounding box labels. Extending ReAL to additional methods and/or annotation tasks (e.g. segmentation) is an interesting direction for future work. As we see on the COCO 2017 dataset in figure 1, our approach has not yet been shown to yield any improvements on artificially balanced and de-cluttered datasets. Our approach is generically useful for any aerial image task; which can have positive or negative social implications depending on the application.

Existing approaches to active learning for detection adopt either an Image-level approach, whereby selected images are exhaustively labeled with desired categories, or an Object-level approach, where single points or regions are sent to an oracle. Both of these can be highly suboptimal in relatively reasonable real-world situations. We introduced a new Region-level approach that subsumes the Image-level and Object-level approaches into a generalized approach that allows region-level selection and promotes spatial-diversity by avoiding nearby redundant queries from the same image. In addition, we developed a novel detector variant of a recently introduced minimax active learning method that balances diversity and uncertainty measures. We show that our approaches significantly decrease labeling effort on natural, real-world data with inherent class-imbalance and cluttered scenes.

References

- [1] Yotam Abramson and Yoav Freund. Active learning for visual object recognition. In *Technical report*. UCSD, 2004. [2](#)
- [2] Hamed H Aghdam, Abel Gonzalez-Garcia, Joost van de Weijer, and Antonio M López. Active learning for deep detection neural networks. In *Proceedings of the IEEE/CVF International Conference on Computer Vision*, pages 3672–3680, 2019. [1](#), [2](#)
- [3] Jordan T. Ash, Chicheng Zhang, Akshay Krishnamurthy, John Langford, and Alekh Agarwal. Deep batch active learning by diverse, uncertain gradient lower bounds. In *Eighth International Conference on Learning Representations (ICLR)*, April 2020. [2](#)
- [4] William H Beluch, Tim Genewein, Andreas Nürnberger, and Jan M Köhler. The power of ensembles for active learning in image classification. In *Proceedings of the IEEE Conference on Computer Vision and Pattern Recognition*, pages 9368–9377, 2018. [2](#)
- [5] Alberto Bietti. Active learning for object detection on satellite images. *Technical report, Technical report, Caltech*, 2012. [2](#)
- [6] Clemens-Alexander Brust, Christoph Käding, and Joachim Denzler. Active learning for deep object detection. *arXiv preprint arXiv:1809.09875*, 2018. [1](#), [2](#)
- [7] Yuxin Chen, Hiroaki Shioi, Cesar Fuentes Montesinos, Lian Pin Koh, Serge Wich, and Andreas Krause. Active detection via adaptive submodularity. In *International Conference on Machine Learning*, pages 55–63. PMLR, 2014. [2](#)
- [8] Sai Vikas Desai and Vineeth N Balasubramanian. Towards fine-grained sampling for active learning in object detection. In *Proceedings of the IEEE/CVF Conference on Computer Vision and Pattern Recognition Workshops*, pages 924–925, 2020. [1](#), [2](#)
- [9] Sai Vikas Desai, Akshay L Chandra, Wei Guo, Seishi Nishimura, and Vineeth N Balasubramanian. An adaptive supervision framework for active learning in object detection. *arXiv preprint arXiv:1908.02454*, 2019. [2](#)
- [10] Sayna Ebrahimi, William Gan, Dian Chen, Giscard Bimby, Kamyar Salahi, Michael Laielli, Shizhan Zhu, and Trevor Darrell. Minimax active learning. *arXiv preprint arXiv:2012.10467*, 2020. [1](#), [2](#), [4](#)
- [11] Marc Gorriz, Axel Carlier, Emmanuel Faure, and Xavier Giro-i Nieto. Cost-effective active learning for melanoma segmentation. *arXiv preprint arXiv:1711.09168*, 2017. [2](#)
- [12] Chieh-Chi Kao, Teng-Yok Lee, Pradeep Sen, and Ming-Yu Liu. Localization-aware active learning for object detection. In *Asian Conference on Computer Vision*, pages 506–522. Springer, 2018. [2](#)
- [13] Ashish Kapoor, Kristen Grauman, Raquel Urtasun, and Trevor Darrell. Active learning with gaussian processes for object categorization. In *2007 IEEE 11th International Conference on Computer Vision*, pages 1–8. IEEE, 2007. [2](#)
- [14] Darius Lam, Richard Kuzma, Kevin McGee, Samuel Dooly, Michael Laielli, Matthew Klaric, Yaroslav Bulatov, and Brendan McCord. xviv: Objects in context in overhead imagery. *arXiv preprint arXiv:1802.07856*, 2018. [4](#), [5](#), [6](#)
- [15] Tsung-Yi Lin, Michael Maire, Serge Belongie, James Hays, Pietro Perona, Deva Ramanan, Piotr Dollar, and Larry Zitnick. Microsoft coco: Common objects in context. In *ECCV. European Conference on Computer Vision*, September 2014. [4](#), [5](#)
- [16] Hieu T Nguyen and Arnold Smeulders. Active learning using pre-clustering. In *Proceedings of the twenty-first international conference on Machine learning*, page 79. ACM, 2004. [2](#)
- [17] Soumya Roy, Asim Unmesh, and Vinay P Nambodiri. Deep active learning for object detection. In *BMVC*, page 91, 2018. [1](#), [2](#)
- [18] Ozan Sener and Silvio Savarese. Active learning for convolutional neural networks: A core-set approach. In *International Conference on Learning Representations*, 2018. [2](#)
- [19] Burr Settles. Active learning literature survey. 2010. *Computer Sciences Technical Report*, 1648, 2014. [6](#)
- [20] H Sebastian Seung, Manfred Opper, and Haim Sompolinsky. Query by committee. In *Proceedings of the fifth annual workshop on Computational learning theory*, pages 287–294, 1992. [2](#)
- [21] Samarth Sinha, Sayna Ebrahimi, and Trevor Darrell. Variational adversarial active learning. In *Proceedings of the IEEE/CVF International Conference on Computer Vision (ICCV)*, October 2019. [2](#)
- [22] D. Wang and Y. Shang. A new active labeling method for deep learning. In *2014 International Joint Conference on Neural Networks (IJCNN)*, pages 112–119, 2014. [2](#)
- [23] Keze Wang, Xiaopeng Yan, Dongyu Zhang, Lei Zhang, and Liang Lin. Towards human-machine cooperation: Self-supervised sample mining for object detection. In *Proceedings of the IEEE Conference on Computer Vision and Pattern Recognition*, pages 1605–1613, 2018. [1](#), [2](#)
- [24] Keze Wang, Dongyu Zhang, Ya Li, Ruimao Zhang, and Liang Lin. Cost-effective active learning for deep image classification. *IEEE Transactions on Circuits and Systems for Video Technology*, 27(12):2591–2600, 2017. [2](#)
- [25] Lin Yang, Yizhe Zhang, Jianxu Chen, Siyuan Zhang, and Danny Z Chen. Suggestive annotation: A deep active learning framework for biomedical image segmentation. In *International Conference on Medical Image Computing and Computer-Assisted Intervention*, pages 399–407. Springer, 2017. [2](#)